AIAA JOURNAL
Vol. 45, No. 5, May 2007

Investigation of Scaled Hypervelocity Gouging Model and Validation of Material Constitutive Models

J. D. Cinnamon,* A. N. Palazotto,† A. G. Szmerekovsky,‡ and R. J. Pendleton§
U.S. Air Force Institute of Technology, Wright–Patterson Air Force Base, Ohio 45433

DOI: 10.2514/1.19940

In an effort to improve the accuracy and validate the performance of a hypervelocity gouging model developed for the shock-wave physics code CTH, the physical dimensionality of an impact problem at the Holloman Air Force Base High-Speed Test Track is mathematically scaled. The resulting scaled impact problem is sized for laboratory experimental testing and modeled. The contact schemes and approaches to friction available in CTH are summarized. In addition, results of a hypervelocity laboratory gouging experiment are presented. CTH is used to model these experimental tests, and the modeling efforts are validated. These efforts enhance the ability of a previously developed full-scale gouging model to be improved and validated.

Nomenclature

C_i	=	arbitrary constants
d	=	diameter of the rod
d_i	=	exponent of the fundamental dimension
E	=	modulus of elasticity
G_o	=	shear modulus of material
L	=	fundamental dimension of length
L_i	=	fundamental dimensions used in the Buckingham Pi theorem
l	=	length of the slipper or rod
M	=	fundamental dimension of mass
m	=	mass of the projectile
q_i	=	dimensioned quantities used in the Buckingham Pi theorem
T	=	fundamental dimension of time
T_m	=	melting temperature
t	=	time of simulation
u_x	=	horizontal velocity
u_y	=	vertical velocity
w	=	width of the slipper
α_i	=	Buckingham Pi exponent
β_i	=	vector of α_i exponents
ν	=	Poisson's ratio
Π	=	overall Buckingham Pi invariant
$\pi_1 - \pi_{10}$	=	invariants
ρ	=	material density
$\sigma_{y,c}$	=	compressive yield strength of the material

I. Introduction

THE Holloman High-Speed Test Track (HHSTT) is a U.S. Air Force test facility that conducts hypervelocity impact testing. The HHSTT performs this testing using rocket-propelled sleds that ride on a 15.5-km steel rail track. The rocket sleds are held on the rails by steel "shoes/slippers." Fig. 1a illustrates the sled and shoe geometry. Current testing capability allows for impact testing at 1–2 km/s, with near-term goals of a velocity greater than 3 km/s. At these velocities, the shoes impact the rail due to the motion experienced by the test sled. The severity of the impact varies, but in certain cases can result in catastrophic failure of the test sled. Inspections of the rails after test events have revealed damage in the form of gouges [1]. Gouges associated with high-energy impacts are characterized by a teardrop-shaped shallow depression in the material (see Fig. 1b). These gouges typically are the result of a high-pressure core developing at the material interface and high viscoplasticity that leads to material mixing (i.e., shoe material becoming embedded within the rail, and vice versa) [1–6].

Simulations of the hypervelocity gouging process have previously been conducted [2–6] using the hydrocode CTH [7,8]. A plane-strain model of the shoe/rail interaction was developed as an accurate, and computationally necessary, representation of the actual impact geometry [2–6]. These previous models were limited by the material constitutive relationships present within the CTH code. Therefore, an effort was undertaken to perform experimentation on the specific materials (VascoMax 300 for the shoes, 1080 steel for the rails) to arrive at accurate constitutive models [9,10]. To validate CTH's ability to simulate the hypervelocity impact of the HHSTT sled shoe and rail, a scaled hypervelocity impact scenario is developed. This is necessitated by our inability to recreate gouging at the HHSTT at a prescribed instrumented point and under measurable impact conditions. Additionally, the cost of each hypervelocity test at the HHSTT precludes us from using the test runs for gouge creation.

Therefore, a laboratory hypervelocity gouge test is developed and the results are presented. CTH is then used to simulate these laboratory impacts and demonstrates good agreement with the experimental results. Through this approach, the constitutive models created thus far are validated and can be applied to the full-scale problem at the HHSTT.

II. Scaled Gouging Test Development

In developing a laboratory hypervelocity gouging scenario in which to examine this phenomenon of gouging and to establish test parameters to simulate within CTH, a mathematical scaling approach was used. The well-known Buckingham Pi technique, which has been applied on this type of problem previously [4,11], was adopted. The goal of this effort was to arrive at test parameters that could be replicated by the gun facility that was available to the authors.

According to the Buckingham Pi theorem, if a physical law consists of a number of quantities $\{q_i\}^m$ that have dimension and are products and powers of j-independent fundamental dimensions L_j, then a unit-free fundamental law can be defined as

Received 8 September 2005; revision received 14 May 2006; accepted for publication 30 May 2006.

*Lieutenant Colonel, U.S. Air Force, Ph.D., Professional Engineer, Adjunct Professor, Department of Aeronautics and Astronautics. Member AIAA.

†Professor, Department of Aeronautics and Astronautics. Fellow AIAA.

‡Lieutenant Colonel, U.S. Air Force, Ph.D., Assistant Professor, Department of Engineering Mechanics, U.S. Air Force Academy. Member AIAA.

§Captain, U.S. Air Force, Department of Aeronautics and Astronautics.

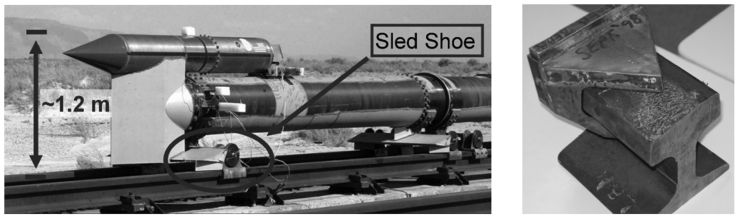

a) b)

Fig. 1 HHSTT system a) sled/shoe geometry and b) shoe/rail section with gouge.

$$f(q_1, q_2, q_3, \cdots, q_m) = 0 \tag{1}$$

where m is the number of dimensioned quantities to be used in the analysis [12]. A fundamental dimension is a quantity that is used to describe a dimensioned quantity. There are many different fundamental systems that can be used, such as force, length, and time (FLT) and mass, length, and time (MLT). Take pressure, for example, in the FLT system, pressure would be represented as FL^{-2}, in the MLT system; pressure is represented as $ML^{-1}T^{-2}$. It must be ensured that the fundamental dimensions alone can describe all dimensioned quantities.

As mentioned earlier, it is possible to represent any dimensioned quantity as a product of fundamental dimensions raised to some power:

$$q_i = [L_1^{d_1}\ L_2^{d_2}\ \cdots\ L_n^{d_n}]_i \tag{2}$$

where q_i is a dimensioned quantity, L_j is a fundamental dimension, and d_k is the power to which the fundamental dimension is raised. The dimensioned quantities can then be combined to form invariant Pi quantities:

$$\Pi = (q_1)^{\alpha_1}\ (q_2)^{\alpha_2}\ \cdots\ (q_m)^{\alpha_m} \tag{3}$$

where α_i is an exponent to be determined. It then follows that

$$\Pi = \left(L_1^{d_1}\ L_2^{d_2}\ \cdots\ L_n^{d_n}\right)_1^{\alpha_1}\left(L_1^{d_1}\ L_2^{d_2}\ \cdots\ L_n^{d_n}\right)_2^{\alpha_2}\cdots\left(L_1^{d_1}\ L_2^{d_2}\ \cdots\ L_n^{d_n}\right)_m^{\alpha_m} \tag{4}$$

Rearranging this equation so that all of the L_i quantities are together leads to

$$\Pi = (L_1)^{\beta_1}\ (L_2)^{\beta_2}\ \cdots\ (L_n)^{\beta_n} \tag{5}$$

where the exponents β can be described as

$$\begin{Bmatrix} \beta_1 \\ \beta_2 \\ \vdots \\ \beta_n \end{Bmatrix} = \begin{bmatrix} d_{11} & d_{12} & \cdots & d_{1m} \\ d_{21} & d_{22} & & d_{2m} \\ \vdots & & \ddots & \vdots \\ d_{n1} & d_{n2} & \cdots & d_{nm} \end{bmatrix} \begin{Bmatrix} \alpha_1 \\ \alpha_2 \\ \vdots \\ \alpha_m \end{Bmatrix} \tag{6}$$

Mathematically, $\{\alpha\}$ must exist in the null space of the dimension matrix $[D]$ for the physical law to be dimensionally consistent. This requires that $\{\beta\} = \{0\}$. This requirement forces the solution of Eq. (6) to give the products of dimensioned quantities that must remain invariant between models [12].

Also according to the theorem, if there are m dimensioned quantities and r fundamental dimensions, then there are $k = m - r$ independent dimensionless quantities. In the MLT system, there will be $r = 3$ fundamental dimensions [12].

Careful selection of the variables to be used within the Buckingham Pi approach is required. Those characteristics, such as material density, which can be expressed as functions of other chosen parameters, are removed from consideration. Because the authors wish to scale the shoe/rail geometry but still experiment with the materials at the HHSTT (VascoMax 300 and 1080 steel), some of the material properties (such as the wave speed of the material) are also removed from consideration. If that was not done, the Buckingham Pi theorem would dictate an experimental test in which two different materials (which result from the scaling of the material properties) could be shot in our laboratory hypervelocity scenario.

It should be noted here that previous modeling of the sled/rail interaction was done in a plane-strain manner [2–6]. This choice and the implications to our scenario will be discussed in detail later in this work. At this point, however, the dimension of width (into the depth of a plane-strain implementation) is removed from consideration. Additionally, the rail dimensions are not scaled, because the rail appears as an infinite half-plane of material to the shoe (or scaled impact projectile) over the timescale of a gouging impact (approximately 10 μs). Therefore, taking the minimum number of fundamental characteristics from the sled/rail geometry, we arrive at the selected dimensioned quantities appearing in Table 1.

With these choices, the invariant parameter Π then becomes

$$\Pi = (m)^{\alpha_1}(l)^{\alpha_2}(d)^{\alpha_3}(u_x)^{\alpha_4}(u_y)^{\alpha_5}(\sigma_{y,c})^{\alpha_6}(E_m)^{\alpha_7}(G_o)^{\alpha_8}(t)^{\alpha_9} \tag{7}$$

In fundamental dimension form, Eq. (4) becomes

$$\Pi = (M)^{\alpha_1}(L)^{\alpha_2}(L)^{\alpha_3}(LT^{-1})^{\alpha_4}(LT^{-1})^{\alpha_5}(ML^{-1}T^{-2})^{\alpha_6}(ML^{-1}T^{-2})^{\alpha_7} \times (ML^{-1}T^{-2})^{\alpha_8}(T)^{\alpha_9} \tag{8}$$

This reduces to

$$\Pi = (M)^{\beta_1}(L)^{\beta_2}(T)^{\beta_3} \tag{9}$$

where $\beta_1 = \alpha_1 + \alpha_6 + \alpha_7 + \alpha_8$, $\beta_2 = \alpha_2 + \alpha_3 + \alpha_4 + \alpha_5 - \alpha_6 - \alpha_7 - \alpha_8$, and $\beta_3 = -\alpha_4 - \alpha_5 - 2\alpha_6 - 2\alpha_7 - 2\alpha_8 + \alpha_9$.

Setting the values of β to zero and solving for $m = \alpha_1$, $l = \alpha_2$, and $u_x = \alpha_4$, one obtains

$$\alpha_1 = -\alpha_6 - \alpha_7 - \alpha_8 \qquad \alpha_2 = -\alpha_3 + 3\alpha_6 + 3\alpha_7 + 3\alpha_8 - \alpha_9$$
$$\alpha_4 = -\alpha_5 - 2\alpha_6 - 2\alpha_7 - 2\alpha_8 + \alpha_9 \tag{10}$$

If these equations are rewritten in vector form, the result is

Table 1 Buckingham Pi Dimensioned Quantities

Dimensioned quantity	Symbol	Fundamental dimensions
Mass	m	M
Height	d	L
Length	l	L
Horizontal velocity	u_x	LT^{-1}
Vertical velocity	u_y	LT^{-1}
Compressive yield strength	$\sigma_{y,c}$	$ML^{-1}T^{-2}$
Elastic modulus	E_0	$ML^{-1}T^{-2}$
Shear modulus	G_0	$ML^{-1}T^{-2}$

$$\begin{Bmatrix}\alpha_1\\ \alpha_2\\ \alpha_3\\ \alpha_4\\ \alpha_5\\ \alpha_6\\ \alpha_7\\ \alpha_8\\ \alpha_9\end{Bmatrix} = \begin{Bmatrix}0\\ -1\\ 1\\ 0\\ 0\\ 0\\ 0\\ 0\\ 0\end{Bmatrix} C_3 + \begin{Bmatrix}0\\ 0\\ 0\\ -1\\ 1\\ 0\\ 0\\ 0\\ 0\end{Bmatrix} C_5 + \begin{Bmatrix}-1\\ 3\\ 0\\ -2\\ 0\\ 1\\ 0\\ 0\\ 0\end{Bmatrix} C_6 + \begin{Bmatrix}-1\\ 3\\ 0\\ -2\\ 0\\ 0\\ 1\\ 0\\ 0\end{Bmatrix} C_7 + \begin{Bmatrix}-1\\ 3\\ 0\\ -2\\ 0\\ 0\\ 0\\ 1\\ 0\end{Bmatrix} C_8 + \begin{Bmatrix}0\\ -1\\ 0\\ 1\\ 0\\ 0\\ 0\\ 0\\ 1\end{Bmatrix} C_9 \tag{11}$$

The columns of Eq. (11) each represent a separate invariant. The invariant is found by associating each dimensioned quantity with its corresponding α value and raising the dimensioned quantity to the power seen in the column vector. In this case, the invariants are given by

$$\Pi = \left(\frac{d}{l}\right)^{C_3}\left(\frac{u_y}{u_x}\right)^{C_5}\left(\frac{\sigma_{y,c}l^3}{mu_x^2}\right)^{C_6}\left(\frac{E_m l^3}{mu_x^2}\right)^{C_7}\left(\frac{G_o l^3}{mu_x^2}\right)^{C_8}\left(\frac{tu_x}{l}\right)^{C_9} \tag{12}$$

The separate invariants are found by setting one $C = 1$ and the others to zero, which gives

$$\pi_1 = \frac{d}{l}, \qquad \pi_2 = \frac{u_y}{u_x}, \qquad \pi_3 = \frac{\sigma_{y,c}l^3}{mu_x^2}, \qquad \pi_4 = \frac{E_m l^3}{mu_x^2}$$
$$\pi_5 = \frac{G_o l^3}{mu_x^2}, \qquad \pi_6 = \frac{tu_x}{l} \tag{13}$$

To maintain proper scaling, these six parameters must be matched in between the HHSTT sled and the developed laboratory hypervelocity impact scenario. Term π_1 of Eq. (13) defines the geometry aspect ratio, π_2 defines the impact angle. Terms π_3 through π_5 relate material properties, length, mass, and horizontal velocity. Parameter π_6 is a timescale that can be used to compare the two scenarios.

Table 2 HHSTT dimensioned quantities [11]

Dimensioned quantity	Symbol	Value
Mass	m	19.1 kg
Height	d	2.54 cm
Length	l	20.32 cm
Horizontal velocity	u_x	1500 m/s
Vertical velocity	u_y	−1 m/s
Compressive yield strength	$\sigma_{y,c}$	14.47 GPa
Elastic modulus	E_0	180.7 GPa
Shear modulus	G_0	70.42 GPa

To scale the HHSTT sled problem, we begin with the known parameters from that gouging scenario. A nominal sled has a mass of 800 kg. The shoes that connect the sled to the rails are generally 20.32-cm long by 10.8-cm wide by 2.54-cm high. Taking a unit slice of the geometry for a plane-strain implementation (again, discussed later), the parameters for the HHSTT become those listed in Table 2.

Using these values for the HHSTT, the invariant parameters from the Buckingham Pi theorem can be computed. Those parameters can then be used in determining the required geometry of a scaled hypervelocity projectile. The π parameters establish ratios between these characteristics. Therefore, to arrive at a design for the laboratory test, we must constrain the solution space with real-world test limitations. Initially, we chose 0.6 cm as the hypervelocity projectile height, which allowed us to generate the remaining values. Unfortunately, this created a scenario that exceeded the capability of the guns available. Consequently, we optimized the available design variables (based on gun limitations) to arrive at the test geometry that best matched the π parameters. The impact angle selected was one that would guarantee gouging, due to a limited number of tests available to the authors. Table 3 summarizes the parameters that results from the HHSTT geometry and the required scaled parameters for the laboratory tests. Parameter π_6 is not presented, because it is used to compare timescales and not geometry.

If strict adherence to the Buckingham Pi approach was possible, the test geometry would have been characterized according to the theoretical column in Table 3. The value of the mathematical determination of the theoretical scaled scenario is that this particular geometry can be shot at some specially equipped test facilities. However, the gun arrangement available to the authors restricted the geometry to projectiles of 4.78-g mass, 5.5-mm diameter, and 25-mm long cylinders with hemispherical noses. The projectiles were limited due to a requirement to be aerodynamically stable in flight and sized for launch by the specific gun hardware. The maximum velocity achievable from our facility was 2225 m/s. As noted previously, this limitation led the authors to increase the impact angle to ensure that sufficient energy was directed into the target rail to generate gouging.

III. Experimental Hypervelocity Gouging Tests

Based on the Buckingham Pi analysis, and constrained by the capability of our laboratory gun facility, the test parameters for a scaled hypervelocity gouging test were chosen. Although matching the π parameters exactly was not possible, an attempt was made to establish a test geometry that reduced the difference between the theoretical π parameters and the experimental π parameters. These values appear in Table 3. The goal, of course, was to generate hypervelocity gouging within a laboratory scenario.

The experimental apparatus was available at the 46th Test Wing, Wright-Patterson Air Force Base, Ohio. The projectile was fired by a 30-mm powder gun, as pictured in Fig. 2. The projectile was held in the barrel by a sectioned sabot that split apart during free flight. The sabot sections hit the "sabot stripper" plate and the projectile traveled through the hole to hit the target rail, as shown in Fig. 3.

The target was set at an angle to the projectile path to establish the impact angle. The impact itself was recorded by two high-speed digital cameras, operating at 47,000 frames per second. Because of a limited number of test shots available, the four test shots were conducted with sufficiently high impact angles to ensure gouge

Table 3 Parameters resulting from Buckingham Pi approach

Parameter	HHSTT scenario	Theoretical scaled scenario	Actual scaled scenario
π_1	.125	.125	.22
π_2	-6.67×10^{-4}	-6.67×10^{-4}	−.1763
π_3	.282	.282	.9851
π_4	35.619	35.619	125.4
π_5	13.984	13.984	48.88
Horizontal velocity	1500 m/s	4809 m/s	2190 m/s
Vertical velocity	−1 m/s	−3.2 m/s	−386 m/s

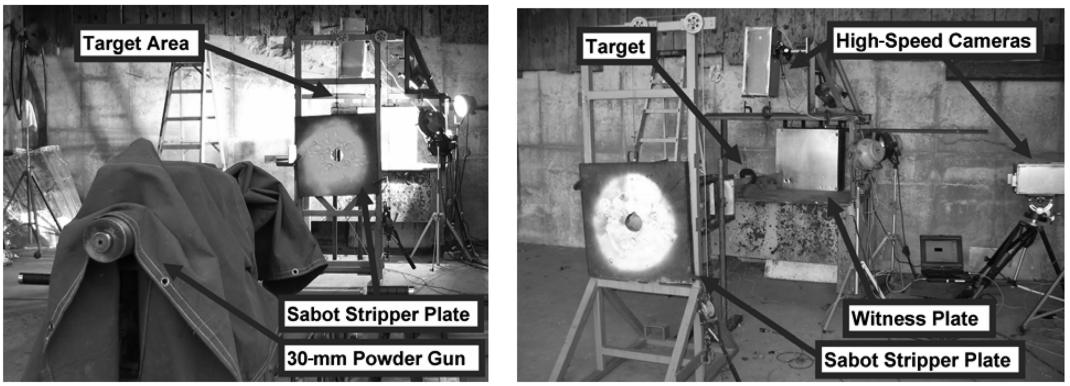

Fig. 2 Experimental test setup.

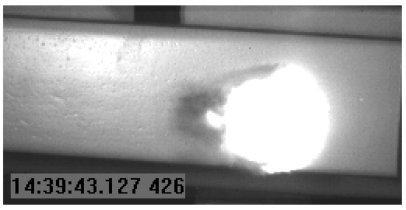

Fig. 3 High-speed photograph of hypervelocity impact on epoxy-coated rail.

generation. Additionally, two target types were shot: one rail with iron-oxide coating and the other with epoxy coating. These are the two coatings in use on the rails at the HHSTT to mitigate the formation of gouging. Table 4 summarizes the test shots and the resulting gouges.

Figure 3 is a high-speed photograph of the impact event. The projectile entered the frame from the left and impacted the epoxy-coated rail surface. The flare generated is associated with viscoplastic material response and indicates the large thermal input into the rail, which was previously reported [1,13]. The VascoMax 300 projectiles fragmented upon impact, making projectile recovery impossible. Figure 4 shows two of the four gouges created in this hypervelocity gouge test. Although beyond the scope of this paper, the gouges were examined metallurgically through the depth, and similar microstructure changes were observed as in previous reports [13–15], which lead us to conclude that these deformed regions are gouges. That is, a large thermal event accompanied by material mixing has occurred.

IV. Examination of CTH Modeling

Efforts to simulate these types of hypervelocity impacts have been conducted for many years [7,8]. One of the most successful codes is the hydrocode CTH. CTH is unique in that it possesses a large body of experimental data embedded in equation-of-state (EOS) tables.

Table 4 Scaled hypervelocity gouge test results

Test	Coating	Angle	Impact velocity	Gouge depth (measured)
hi-1	Oxide	10 deg	2225 m/s	0.5 ± 0.1 mm
hi-2	Oxide	15 deg	2150 m/s	1.0 ± 0.1 mm
he-1	Epoxy	15 deg	2147 m/s	1.0 ± 0.1 mm
he-2	Epoxy	10 deg	2163 m/s	0.5 ± 0.1 mm

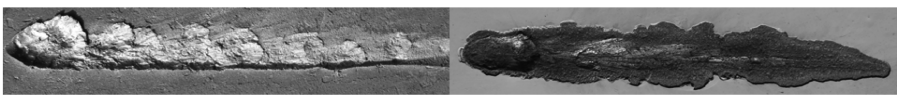

a) b)

Fig. 4 Gouges on target rails: a) iron-oxide-coated rail and b) epoxy-coated rail.

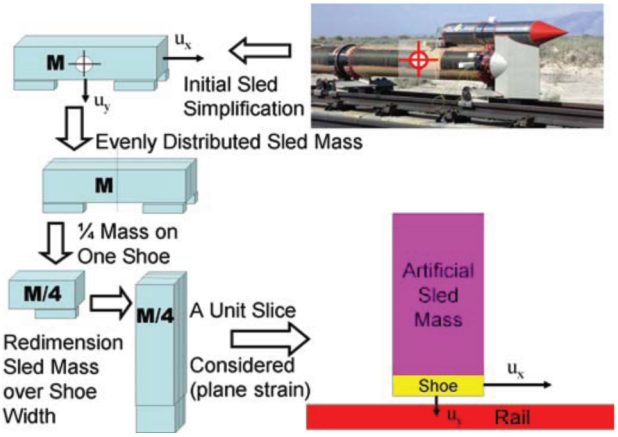

Fig. 5 Development of a plane-strain gouging model [6].

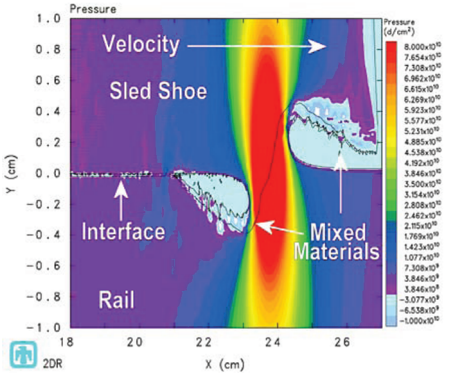

Fig. 6 Typical CTH gouge simulation.

Additionally, CTH was written as a shock-physics code for which the primary purpose is to simulate high-energy impact events [7,8]. The primary limitation of this code is that it is extremely computationally intensive. Users of CTH typically create state-of-the-art computer clusters or use time on some of the nation's fastest supercomputers to have the computation time stay in the reasonable range. A simple problem implemented in full 3-D with all of the associated subroutines engaged can exceed the capability of CTH to simulate the event or local data storage capacity. The mesh size found to show

Table 5 Model constants for VascoMax 300 and 1080 steel

Property	1080 steel	VascoMax 300
A ($\Delta\sigma'_G + kl^{-1/2}$), GPa	0.825	1.42
c_1, GPa	4.0	4.0
c_2, GPa	0	0
c_3, eV^{-1}	160.0	79.0
c_4, eV^{-1}	12.0	3.0
c_5, GPa	0.266	0.266
n	0.289	0.289

a converged solution (0.002 cm) also contributes to the intense computational load to simulate these impacts in 3-D. Finally, simulation times can be as long as two weeks to generate 10 μs of data. Therefore, many users model these impact problems in plane-strain or 2-D axisymmetric models to reduce computation time to the order of tens of hours or days.

With regard to the specific impact problem at the HHSTT, previous researchers performed a comparison between simulating the shoe/rail interaction in 2-D plane strain versus a full 3-D

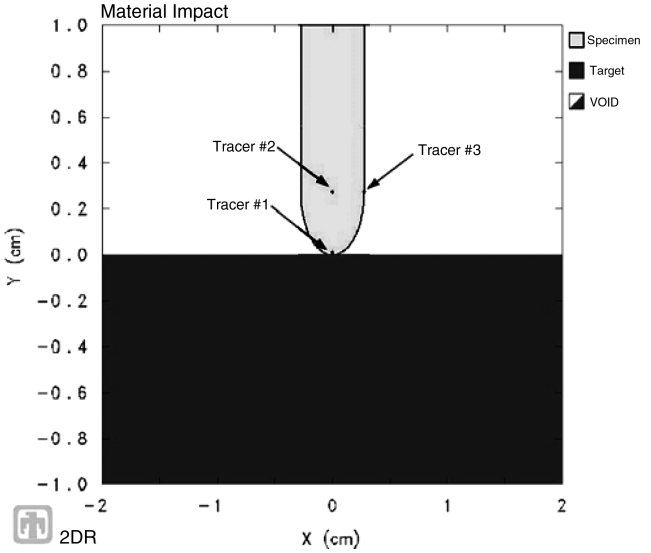

Fig. 7 CTH solution comparison model.

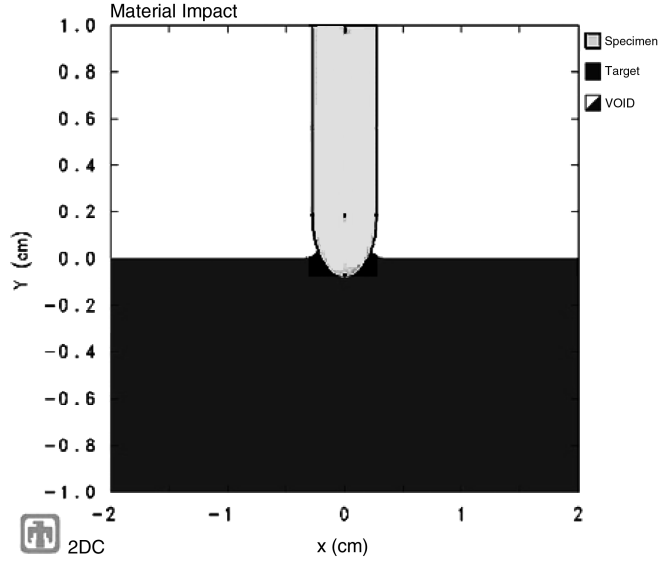

a)

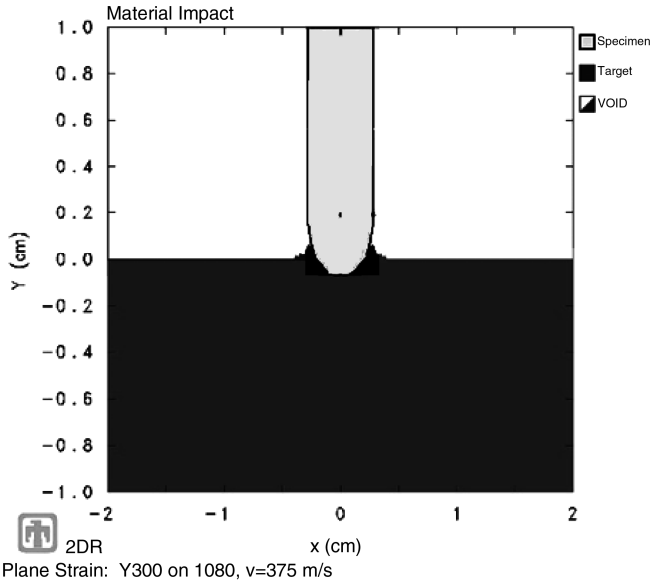

b)

Fig. 8 Solutions at 2.5 μs: a) axisymmetric and b) plane-strain.

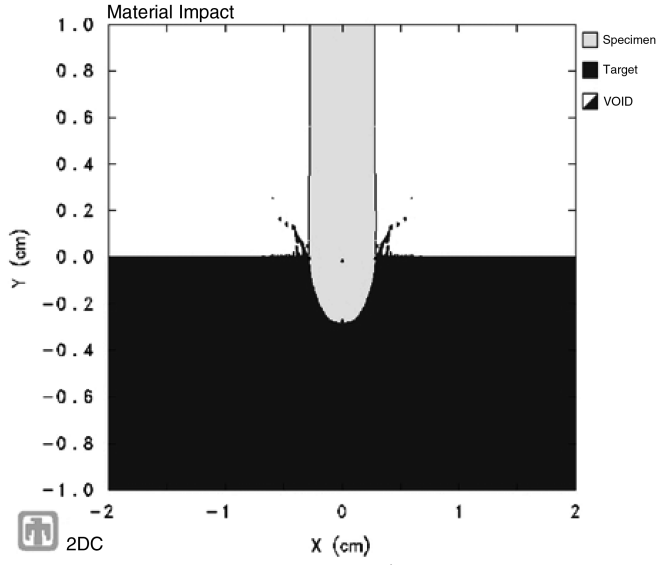

a)

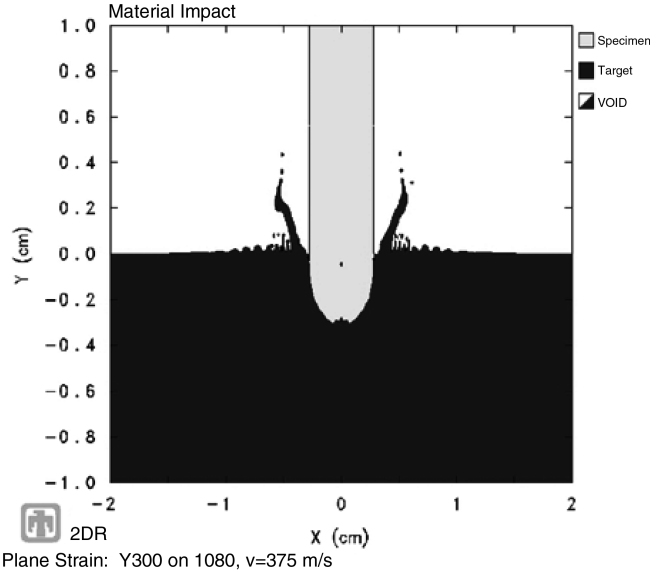

b)

Fig. 9 Solutions at 10 μs: a) axisymmetric and b) plane-strain.

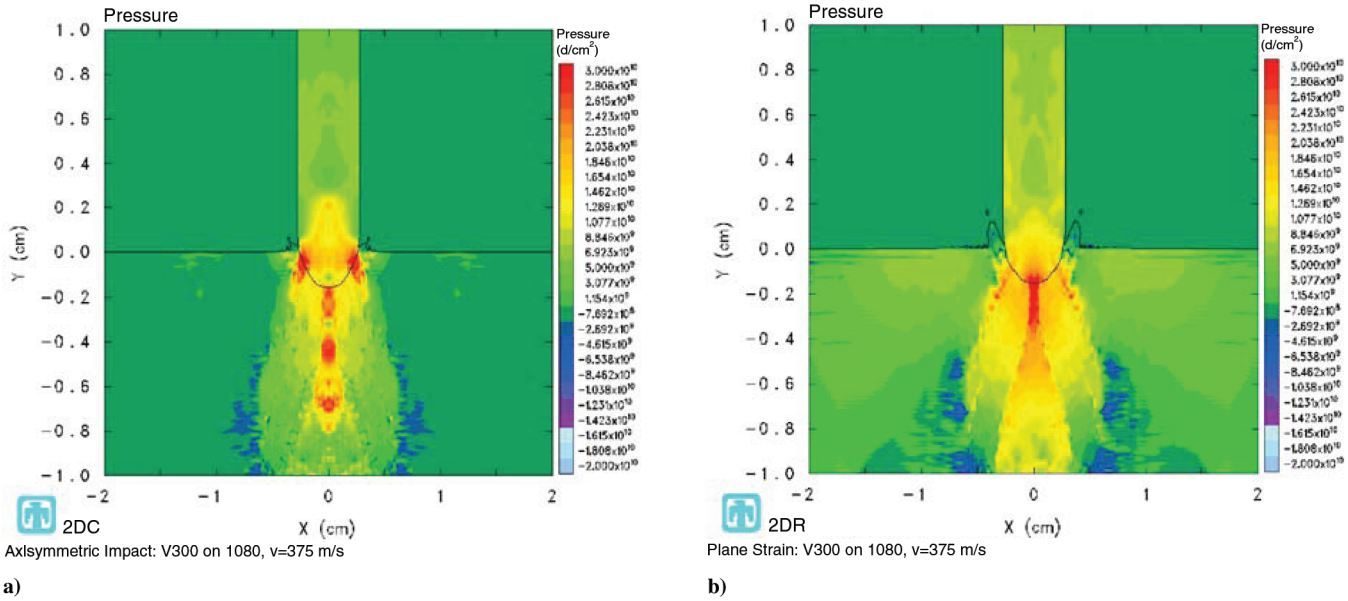

Fig. 10 Solutions at 2.5 μs: a) axisymmetric and b) plane-strain.

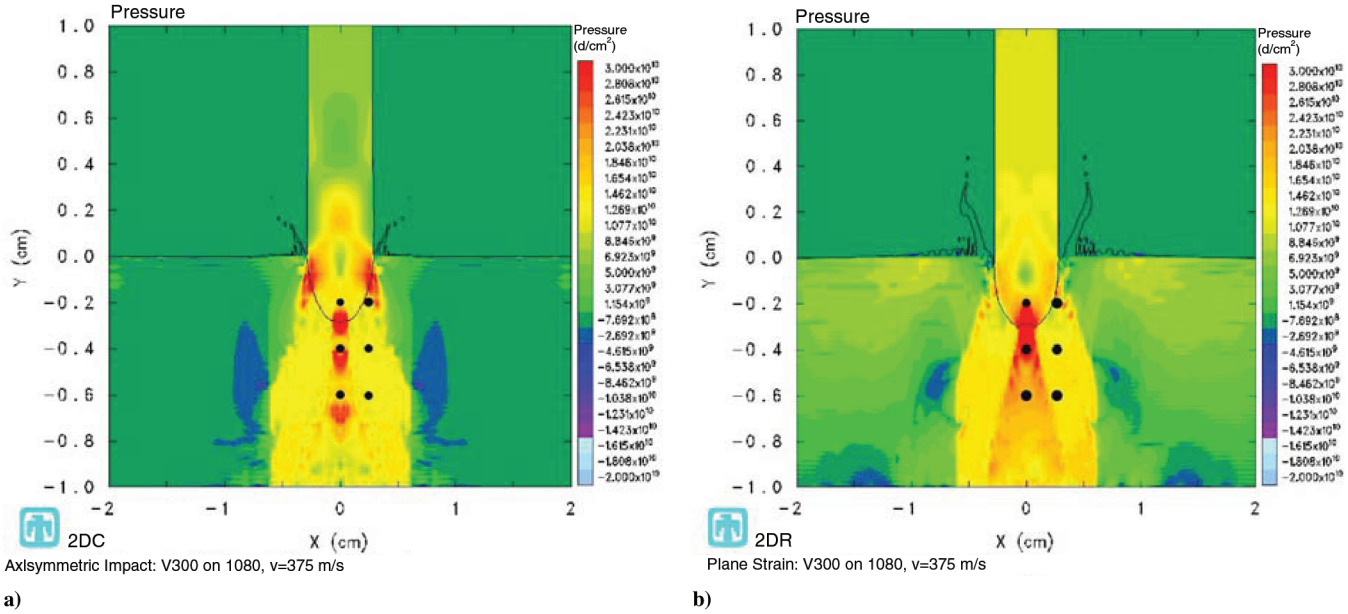

Fig. 11 Solutions at 10 μs: a) axisymmetric and b) plane-strain.

implementation [3]. The conclusion was drawn that a plane-strain version of the impact event was significantly similar to the results from a 3-D solution for a limited period of time [3]. Based on this analysis, subsequent model development was done in plane strain.

Szmerekovsky [4–6] developed a 2-D plane-strain model of the shoe/rail interaction by taking the sled arrangement and distributing the mass of the sled across the four shoes. The mass is then taken to distribute evenly through the width of the shoe, and a unit slice is removed and modeled. This process is depicted in Fig. 5. This model was used very successfully to model the gouging phenomenon. Many of the features observed in the field and from experimental analysis of the gouges were generated by this plane-strain model in CTH. Figure 6 illustrates a typical gouge created in CTH. Material mixing is created and represents one of the unique capabilities of this

Table 6 Pressure comparison, plane strain compared against axisymmetric solution

Discrete point, x coordinate	Discrete Point, y coordinate	% difference, $t = 5$ μs	% difference, $t = 10$ μs
0	−0.2 cm	21%	16%
0	−0.4 cm	9%	14%
0	−0.6 cm	0%	16%
.25 cm	−0.2 cm	17%	30%
.25 cm	−0.4 cm	47%	0%
.25 cm	−0.6 cm	36%	12%
	Average:	31%	14%

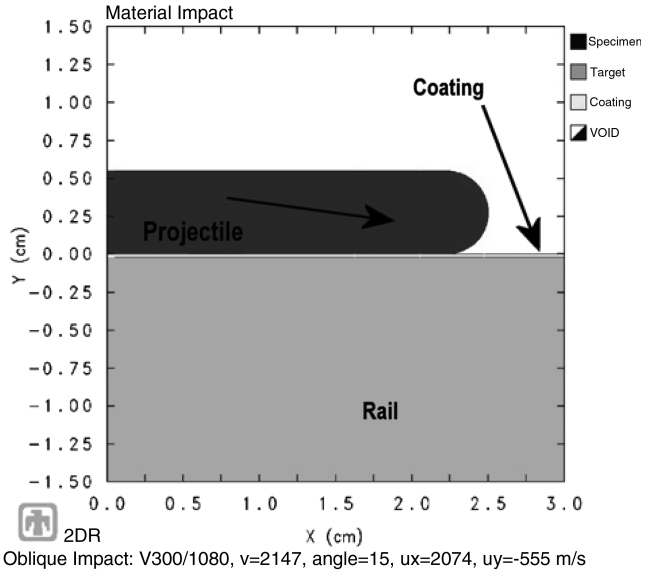

Fig. 12 CTH model of hypervelocity gouging test, with velocity vector depicted.

code. Based on the success of these plane-strain models, and the unreasonable computation times of 3-D implementations, the authors have elected to model these impact events in 2-D plane strain.

As mentioned previously, the major limitation of these modeling efforts to date is the lack of specific material models in CTH for VascoMax 300 and 1080 steel. Although suitable EOS models exist, the constitutive models governing the strength of the materials below EOS pressures are not available. Therefore, an extensive effort was undertaken to develop these material strength models [9,10,14]. To validate these material models, experimental Taylor impact tests were conducted [10,14]. The focus of this current work is to extend the validation into the hypervelocity impact regime.

Related to the previous validation of the strength models in CTH, using the Taylor impact tests, an evaluation of the suitability of 2-D simulations was performed. In previous work, a 2-D model was able to match posttest geometry of the Taylor impact test within 2% (which involves a cylinder of material impacting a nondeforming target at velocities around 200 m/s) [10,14]. Additionally, because of the nature of CTH's development, some additional features have been added to the code for specific reasons. An evaluation of the three material contact schemes was undertaken, and the most numerically stable option was identified (designated as the no-slide line option within CTH) [16].

As previously mentioned, in modeling our hypervelocity gouging tests, we are limited to choosing between plane strain and a full 3-D model. CTH does have a 2-D axisymmetric mode, but it is limited to a vertically oriented impact (normal incidence angle), because it established a vertical line of symmetry and rotates a user-defined 2-D slice about it. Motivated by previous success in 2-D modeling, the authors in this work decided to investigate the difference between this axisymmetric mode and a plane-strain mode solution of impact problems.

For this examination, a penetration model was created based on our hypervelocity experimentation. The projectiles used in our gun tests were modeled to impact the rail at a normal incidence angle and at the velocity range corresponding to the vertical impact velocity of our hypervelocity shots (i.e., 375–555 m/s). The material flow relation used in our modeling was the Zerilli–Armstrong model [17]. The material model constants were formulated from flyer plate experiments in a related study [18]. Table 5 summarizes the material model constants used within CTH. The temperature constants c_3 and c_4 are given in electron volts.

An axisymmetric model was compared against a plane-strain model of the same vertical impact. The impact geometry is depicted in Fig. 7. The mesh size used was 0.01 cm, which was arrived at by a previous mesh convergence study [5]. In this work, a representative case is examined, in which the projectile hits the target at 375 m/s. Figures 8 and 9 compare the axisymmetric solution to the plane-strain solution at discrete times. Note that the penetrator deformation and penetration depth are in good agreement out to 10 μs, which corresponds both to the event time of the hypervelocity gouging impact test and the gouge event in the HHSTT scenario.

In examining the difference in cell (hydrostatic) pressure generated in each of the solution techniques, six Lagrangian grid points were selected and the pressure was recorded at discrete points of time. Figures 10 and 11 illustrate the pressure profiles, in which the black points in Fig. 11 indicate the points for which the hydrostatic pressure was compared. Although there appears to be some general differences in appearance, the magnitude of the pressure variance is not excessively significant. For the duration of time examined, reflected waves do not return to the area of interest and affect the solution. Table 6 records the pressure differences at each point and summarizes the results.

So although there is some measurable difference between the solution techniques, the magnitude of the difference is not

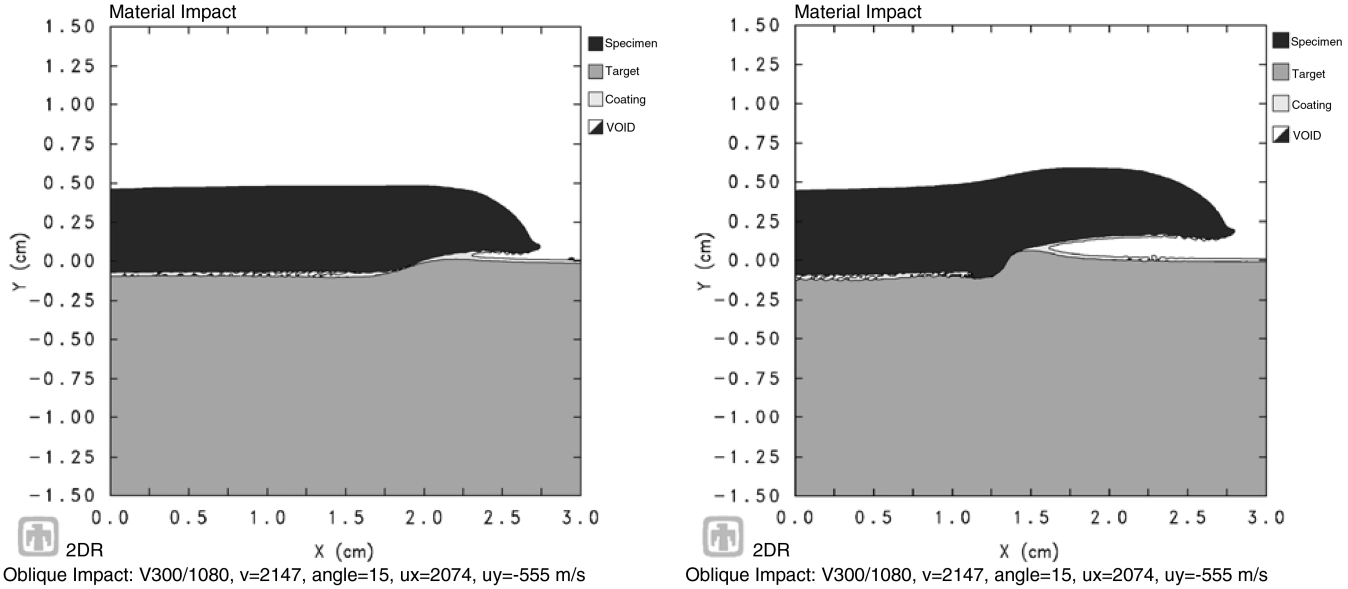

a) **b)**

Fig. 13 Simulation of test he-1 at a) 5 μs and b) 10 μs.

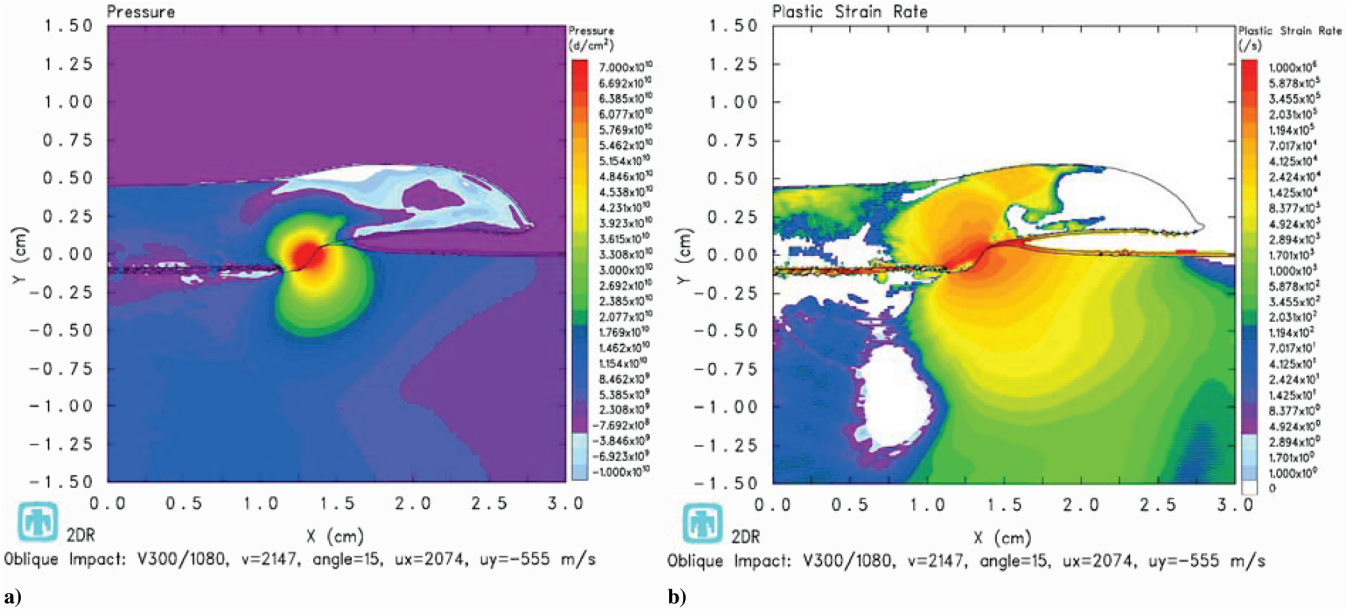

Fig. 14 Test he-1 at 10 μs: a) cell pressure and b) strain rate.

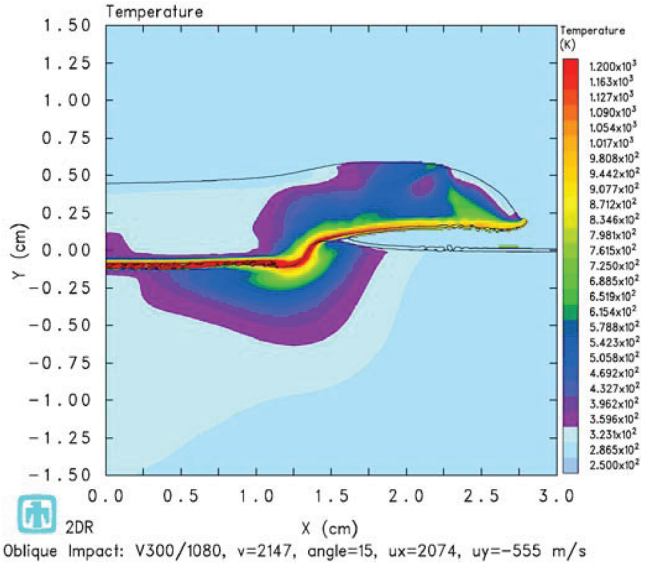

Fig. 15 Temperature profile of test he-1 at 10 μs.

significant. Additionally, the gross deformation predicted by the methods match very well. Note that in Fig. 11, the penetrators are almost identical in diameter (0.26 cm for axisymmetric, 0.25 cm for plane strain, for a difference of 3.8%). Additionally, the penetration depth for both cases is also comparable (0.29 cm for axisymmetric, 0.3 cm for plane strain, for a difference of 3.4%). Even better agreement was noted in the 555 m/s impact case. Based on this evaluation, we conclude that the plane-strain solution technique can fairly accurately model this 3-D impact event for a short length of time. The authors would employ the 2-D axisymmetric model for the modeling of our laboratory hypervelocity gouging test, but our impact geometry is not compatible with the implementation in CTH.

V. Validation of the Material Models Using Laboratory Hypervelocity Gouging Tests

With the investigation presented earlier, the authors constructed a 2-D plane-strain model of the hypervelocity gouging test. Using this approach, the cylinder with a hemispherical nose is modeled as a unit-thickness plate with a rounded leading edge. Figure 12 illustrates this model. The high-speed photography available from the impacts indicated that the projectile oriented during flight in such a manner as to impact the target rail, as depicted in Fig. 12. Although the velocity vector was still oriented at 10 or 15 deg to the rail surface, the long axis of the projectile was aligned with the longitudinal axis of the target rail.

Again, the appropriate mesh size was used [5]. All four impact cases were examined. A representative case is presented in this paper. Figure 13 is of impact test he-1, with an impact velocity of 2147 m/s, and an impact angle of 15 deg. The solution shows the characteristic material mixing and high plasticity of gouging. Additionally, Fig. 14 illustrates the pressure and strain rate associated with 10 μs.

The four simulations demonstrated good agreement to experimentally observed values for gouge depth. Table 7 summarizes these results; note that simulated depths are within the experimental measurement uncertainty.

The characteristics of hypervelocity gouging discussed earlier, such as a high-pressure concentration [4,5] at the gouge location and material mixing, are evident in these simulations. Additionally, localized temperature (illustrated in Fig. 15) were generated that could create the microstructural changes reported in the literature [13,14,18].

The goal of these experiments and simulations was to validate the new material models for VascoMax 300 and 1080 steel for use in CTH. The hypervelocity gouging tests were as close, in a laboratory sense, as the authors could get to the conditions at the HHSTT. The plane-strain simulations show outstanding agreement to the experimental tests. This success, compared with earlier efforts, can be attributed to a new strength model that incorporates experimental flyer plate data with strain rates on the order of 10^5/s [18].

Table 7 CTH gouge simulation comparison to experiment

Test	Coating	Angle	Impact velocity	Gouge depth (measured)	Gouge depth (simulated)
hi-1	Oxide	10 deg	2225 m/s	0.5 ± 0.1 mm	0.6 mm
hi-2	Oxide	15 deg	2150 m/s	1.0 ± 0.1 mm	1.1 mm
he-1	Epoxy	15 deg	2147 m/s	1.0 ± 0.1 mm	1.1 mm
he-2	Epoxy	10 deg	2163 m/s	0.5 ± 0.1 mm	0.5 mm

VI. Conclusions

In this work, a scaled laboratory gouging scenario was developed to validate both new material models of the specific steels used at the HHSTT and the hydrocode CTH's ability to simulate these events. An optimization was conducted to match what the available gun range could provide to the theoretical scaled gouging test. A series of scaled hypervelocity gouging tests were conducted, constrained by the gun range capability. In these tests, gouging impacts were recreated.

A discussion of previous modeling efforts in CTH was conducted, with a justification provided for plane-strain depictions of the HHSTT shoe/rail gouging phenomenon. A detailed examination of the difference between a 2-D plane-strain and a 2-D axisymmetric impact model was undertaken. The plane-strain simulations showed good agreement with the axisymmetric model for a limited period of time.

The scaled hypervelocity impact test was then modeled in CTH, using a plane-strain formulation. This modeling effort matched the experimental results very well. The previously reported characteristics of hypervelocity gouging were replicated. This study validated the material models' ability to match experimental gouging results. Additionally, the results indicate the validity of simulating these short-duration events in a plane-strain manner using CTH.

Acknowledgements

The authors would like to acknowledge the support of the U.S. Air Force Office of Scientific Research (Neal Glassman and John Schmisseur, monitors). Also, Mike Hooser from the Holloman High-Speed Test Track made critical contributions to this endeavor. Additionally, the technical advice of Ted Nicholas of the U.S. Air Force Institute of Technology was instrumental to the research.

References

[1] Gerstle, F. P., Follansbee, P. S., Pearsall, G. W., and Shepard, M. L., "Failure of Steel During High Velocity Sliding," *Wear*, Vol. 24, 1973, pp. 97–106.

[2] Laird, D. J., and Palazotto, A. N., "Effects of Temperature on the Process of Hypervelocity Gouging," *AIAA Journal*, Vol. 41, No. 11, 2003, pp. 2251–2260.

[3] Laird, D. J., and Palazotto, A. N., "Gouge Development During Hypervelocity Sliding Impact," *International Journal of Impact Engineering*, Vol. 30, No. 2, 2004, pp. 205–223.

[4] Szmerekovsky, A. G., Palazotto, A. N., and Baker, W. P., "Scaling Numerical Models for Hypervelocity Test Sled Slipper-Rail Impacts," *International Journal of Impact Engineering*, Vol. 32, No. 6, 2006, pp. 928–946.

[5] Szmerekovsky, A. G., Palazotto, A. N., and Earnst, M. R., "Numerical Analysis for a Study of the Mitigation of Hypervelocity Gouging," *Proceedings of the 45th AIAA/ASME/ASCE/AHS/ASC Structures, Structural Dynamics, and Materials Conference*, AIAA, Reston, VA, 2004, pp. 1–10.

[6] Szmerekovsky, A. G., and Palazotto, A. N., "Structural Dynamic Considerations for a Hydrocode Analysis of Hypervelocity Test Sled Impacts," *AIAA Journal*, Vol. 44, No. 6, pp. 1350–1359, 2006.

[7] Hertel, E. S., "CTH: A software family for multidimensional shock physics analysis," *Proceedings of the 19th International Symposium on Shock Waves*, Springer–Verlag, New York, Vol. 1, 1993, pp. 377–382.

[8] McGlaun, J. M., Thompson, S. L., and Elrick, M. G., "CTH: A Three-Dimensional Shock Wave Physics Code," *International Journal of Impact Engineering*, Vol. 10, Nos. 1–4, 1990, pp. 351–360.

[9] Cinnamon, J. D., Palazotto, A. N., Brar, N. S., Kennan, Z., and Bajaj, D., "Johnson-Cook Strength Model Constants for Vascomax 300 and 1080 Steels," *Proceedings of the 14th American Physical Society (APS) Topical Conference on Shock Compression of Condensed Matter*, Vol. 845, American Physical Society, College Park, MD, 2006, pp. 709–712.

[10] Cinnamon, J. D., Palazotto, A. N., and Kennan, Z., "Material Characterization and Development of a Constitutive Relationship for Hypervelocity Impact of 1080 Steel and Vascomax 300," *International Journal of Impact Engineering*, Vol. 33, Nos. 1–12, 2006, pp. 180–189.

[11] Rickerd, G. S., Palazotto, A. N., and Cinnamon, J. D., "Investigation of a Simplified Hypervelocity Gouging Model," *46th AIAA/ASME/ASCE/AHS/ASC Structures, Structural Dynamics, and Materials Conference*, AIAA, Reston, VA, 2005, pp. 1–10.

[12] Çengel, Yungas A., and Cimbala, John M., *Fluid Mechanics: Fundamentals and Applications*, McGraw–Hill, Boston, 2006, pp. 282–288.

[13] Cinnamon, J. D., and Palazotto, A. N., "Metallographic Examination of Thermal Effects in Hypervelocity Gouging," *Proceedings of the ASME Pressure Vessels and Piping Conference—2005*, American Society of Mechanical Engineers, New York, 2005, pp. 1–9; also American Society of Mechanical Engineers Paper PVP2005-71613.

[14] Cinnamon, J. D., and Palazotto, A. N., "Refinement of a Hypervelocity Model for the Rocket Sled Test," *Proceedings of the ASME Heat Transfer Division—2005*, American Society of Mechanical Engineers, New York, 2005, pp. 1–10; also American Society of Mechanical Engineers Paper IMECE2005-80004.

[15] Cinnamon, J. D., and Palazotto, A. N., "Metallographic Examination and Validation of Thermal Effects in Hypervelocity Gouging," *Journal of Pressure Vessel Technology*, Vol. 129, No. 1, 2006, pp. 133–141.

[16] Nguyen, M. C., Palazotto, A. N., and Cinnamon, J. D., "Analysis of Computational Methods for the Treatment of Material Interfaces," *46th AIAA/ASME/ASCE/AHS/ASC Structures, Structural Dynamics, and Materials Conference*, AIAA, Reston, VA, 2005, pp. 1–13.

[17] Zerilli, F. J., and Armstrong, R. W., "Dislocation-Mechanics-Based Constitutive Relations for Material Dynamics Calculations," *Journal of Applied Physics*, Vol. 61, No. 5, Mar. 1987, pp. 1816–1825.

[18] Cinnamon, J. D., Palazotto, A. N., and Brar, N. S., "Further Refinement of Material Models for Hypervelocity Gouging Impacts," *47th AIAA/ASME/ASCE/AHS/ASC Structures, Structural Dynamics, and Materials Conference*, AIAA, Reston, VA, 2006, pp. 1–10.

A. Roy
Associate Editor